Journal of Power Sources 613 (2024) 234884

Contents lists available at ScienceDirect

Journal of Power Sources

journal homepage: www.elsevier.com/locate/jpowsour

Comprehensive study of the aging knee and second-life potential of the Nissan Leaf e+ batteries

Wei Gao [a,**], Zhi Cao [a], Yuhong Fu [a], Christopher Turchiano [b], Naser Vosoughi Kurdkandi [a], Jing Gu [b], Chirs Mi [a,*]

[a] Department of Electrical and Computer Engineering, San Diego State University, San Diego, CA, 92182, USA
[b] Department of Chemistry and Biochemistry, San Diego State University, San Diego, CA, 92182, USA

HIGHLIGHTS

- Battery aging knee can be avoided by improving the operating conditions.
- The second life window after the knee point is 75 %~50 % SOH.
- The estimated second life is 4000~6000 cycles and 11–16 years.
- The graphite exfoliation on the anode is the reason of aging knee.

ARTICLE INFO

Keywords:
Aging knee
Second life battery
Echelon utilization
Gas generation
Battery swelling
Battery aging

ABSTRACT

Aging knee may induce rapid degradation of lithium-ion batteries (LIBs) and pose safety risks. It is crucial to study the battery aging knee and find solutions to address it. In this light, this study focuses on the comprehensive aging characterizations of the Nissan Leaf third generation (Gen3) LIBs to elucidate their aging trajectories. Twenty-four battery cells were divided into six groups and cycled at different working conditions, i.e., voltage, current, and temperatures. The test result shows that the batteries tend to reach the aging knee around 75 % state of health (SOH). Then, we improved the working conditions after the knee point to mimic second-life operation. Key findings show that the aging knee can be stopped by improving the working conditions. The battery capacity degradation slowed down to about 4 % per 1000 cycles, projecting a second-life potential of 4000–6000 cycles between 75 % and 50 % SOH. Post-mortem analysis indicated that negative electrode failure is the cause of aging knee and gas generation. The impact of working conditions on the battery aging is analyzed. Based on the analysis, we propose strategies for both the first and second life operations of LIBs to improve battery life and avoid the aging knee.

1. Introduction

The penetration of electric vehicles (EVs) has been increasing fast in recent years. More than 14 million EVs and plug-in hybrid vehicles (PHEVs) were sold globally in 2023, representing 16 % of the market share of all vehicles sold. The predicted EV and PHEV sales in 2035 is 60 million [1]. Tens of millions of EV battery packs (hundreds of GWh) will be retired every year after 8–15 years of operation [2–4]. Second-life utilization of these batteries is believed to be the most economical and environmentally friendly solution compared to direct material recycling [2,5,6].

However, there are many challenges and uncertainties facing second-life batteries (SLBs) [7]. How long can second-life batteries last in battery energy storage systems (BESS) is unknown. The second-life aging trajectory, optimal working conditions, and safety risks are also unclear. Especially with the development of high-nickel [8,9], cobalt-free [10], and silicon/carbon anode LIBs [11], the risk of aging knee and gas generation is higher [12,13], which further increases the uncertainty of SLB utilization.

Aging knee is one of the biggest concerns in using SLBs, after which

* Corresponding author.
** Corresponding author.
E-mail addresses: wgao2@sdsu.edu (W. Gao), cmi@sdsu.edu (C. Mi).

https://doi.org/10.1016/j.jpowsour.2024.234884
Received 16 February 2024; Received in revised form 4 June 2024; Accepted 10 June 2024

batteries exhibit rapid, nonlinear degradation and then die quickly [14]. Some authors claimed that the batteries should not be used after the knee point for safety concerns [2,15]. Under this assumption, a large number of retired EV battery packs with aging knee issues have no second-life value. However, on the contrary, if the aging knee can be prevented or stopped, then tens of millions of retired EV battery packs could be used for a second life, thus providing substantial economic and environmental benefits. Therefore, it is crucial to study the battery aging knee and figure out whether it can be prevented or stopped, and how to realize it.

Recent literature has studied the mechanism of LIB aging knee. Attia et al. [14] summarized six pathways that can cause aging knee: lithium plating, electrode saturation, resistance growth, electrolyte and additive depletion, percolation-limited connectivity, and mechanical deformation. The aging knee was observed on batteries of various positive electrode chemistries, including $LiNi_{1/3}Mn_{1/3}Co_{1/3}O_2$ (NMC111) [16,17], $LiNi_{0.6}Mn_{0.2}$-$Co_{0.2}O_2$ (NMC622) [18], $LiFePO_4$ [19], $LiCoO_2$ [20], and $LiMn_2O_4$/NMC111 blend [21]. Yang et al. [4] claimed that the aging knee is attributed to the sharp rise of lithium plating caused by solid electrolyte interphase (SEI) growth. Schuster et al. [16] found the aging knee may originate from SEI growth and graphite material loss. Scanning electron microscopy (SEM) images showed thick films on the negative electrode, while no obvious change on the positive electrode. Some literature also observed a large amount of metallic lithium on the negative electrode [22]. Therefore, the studies suggest that the aging knee is related to negative electrode material failure.

Some literature proposed algorithms to predict the aging knee [4,23–28], aiming to remind the user to replace the battery to reduce safety risks [15]. Few studies have attempted to find ways to avoid the aging knee to prolong battery life. Schuster et al. [16] claimed that an optimized operational strategy, i.e., 0.2C current, 0.94V voltage range, and 35 °C temperature, may retard the knee. However, this study did not explain how long the batteries can last for a second life, and the 35 °C optimal temperature disagrees with other studies, which found the optimal temperature to be 20 °C–25 °C [2,13,29–31].

The mechanism of LIB gas generation has been studied [32–35]. Literature shows that CO, H_2, and C_2H_4 evolution are related to electrolyte decomposition on the negative electrode, while CO_2 comes from positive electrode decomposition [32]. However, most studies focused on the gas composition and generation [33,35–37] instead of finding solutions to avoid it.

Nissan Leaf was one of the first mass-produced EVs using LIBs. The first generation (Gen1) LiM_2O_4 batteries show a linear aging trajectory until the capacity degrades to 40 % [3,38,39]. However, with the increase of energy density, premature failure, and swelling issues were reported for the 40 kWh and 62 kWh Gen3 battery packs [40]. To study the battery aging knee and find solutions to address it, this study conducted a comprehensive aging test on 24 Nissan Leaf Gen3 batteries. The primary goal is to investigate if the aging knee can be avoided or stopped, and if so, how to achieve it. Then, the battery aging trajectory is illustrated, which provides a clear second-life evaluation. The impact of working conditions on battery aging is studied. Based on the analysis, we propose guidelines for both the first life EV operation and second life BESS operations of LIB to improve battery life. This study provides valuable suggestions for Nissan and other EV manufacturers to avoid battery premature degradation. It also clarifies the prospect of second-life utilization of LIBs with aging knee issues.

The remainder of this paper is organized as follows: In Section 2, the battery aging test is introduced. In Section 3, the particle swarm optimization (PSO) based battery parameter identification is described. In Section 4, the battery post-mortem analysis is demonstrated. In Section 5, the battery aging trajectory, second life evaluation, optimal working condition, gas generation, etc., are analyzed. Conclusions are drawn in Section 6.

2. Experimental setup

2.1. Specification of the Nissan Leaf e + batteries

Nissan Leaf e+ was introduced to the market in 2019. It was equipped with a 62 kWh battery pack (59 kWh useable), which is the third generation (Gen3) LIB designed by Nissan. The EPA mile range is 364 km (226 miles). The peak power of the electric motor is 160 kW (2.7C discharge), while the DC fast charging can reach 70 kW–100 kW (1C–1.7C).

The positive electrode material is LiNMC and the negative electrode material is graphite. The specifications are listed in Table 1 [41]. Compared to its 24 kWh and 30 kWh predecessors [3], the battery cell energy density increased from 157 Wh/kg and 188 Wh/kg to 224 Wh/kg, while the pack energy density increased from 81.6 Wh/kg and 95.2 Wh/kg to 143.9 Wh/kg. The battery pack consists of 288 battery cells, with three connected in parallel and 96 in series (3P–96S). A retried battery module (3P–9S) was sourced from Nissan, as shown in Fig. 4(a), and it was disassembled into 27 battery cells for the battery aging test. The initial SOH was about 89 %. A battery's SOH usually includes capacity degradation and impedance increase. For ease of discussion, in this paper, SOH is defined as the ratio of current battery capacity C_B to its nominal capacity C_n, while the ohmic resistance R_0 and diffusion resistance R_1 are used to represent battery impedance.

2.2. Battery testing systems

Fig. 1 shows the battery aging test system. A Chroma 17010 battery cell tester with 24 channels was used for the battery aging test. The test voltage of each channel is 0V∼5V, and the maximum current is 100A. A CSZ Plus 8 and a THERMOTRON thermal chamber were used to test the batteries at 35 °C and 10 °C, respectively. It is well known that 20 °C–25 °C is ideal for battery operation [13,29]. Subzero temperatures should be avoided because they can induce lithium plating. Therefore, the 0 °C–20 °C temperature range is worthy of study. Here, 10 °C was chosen for the low temperature test to observe its impact on battery aging.

2.3. Battery aging test procedure

The battery aging test consists of four stages, as listed in Table 2. All the batteries were cycled at the same test conditions in the first 240 cycles to validate their performance consistency. In Stage 2, the 24 batteries were divided into six groups and cycled at different test conditions until the aging knee appeared. Then, the batteries were transferred to improved test conditions to mimic second life operation in Stages 3 and 4.

Fig. 2 shows the battery aging test data at different stages. Each aging test process consists of N aging cycles at the specified test conditions followed by four characteristic test cycles. The aging cycle number N would be changed accordingly. For example, considering the fast capacity degradation at the beginning of the aging test, N was set to six to shorten the characteristic test interval. Then, N was increased to 56 after the battery aging speed was stabilized. The cycling data was recorded at a 5 s time step.

The four characteristics test cycles are used to evaluate the battery

Table 1
Specification of the Nissan Leaf Gen 3 battery cell.

Capacity	56.3Ah
Voltage Range	2.8V–4.2V (3.65V Nominal)
Weight	914g
Cell Energy Density	460 Wh/L
Cell Specific Energy	224 Wh/kg
Pack Specific Energy	59 kWh/410 kg = 143.9 Wh/kg

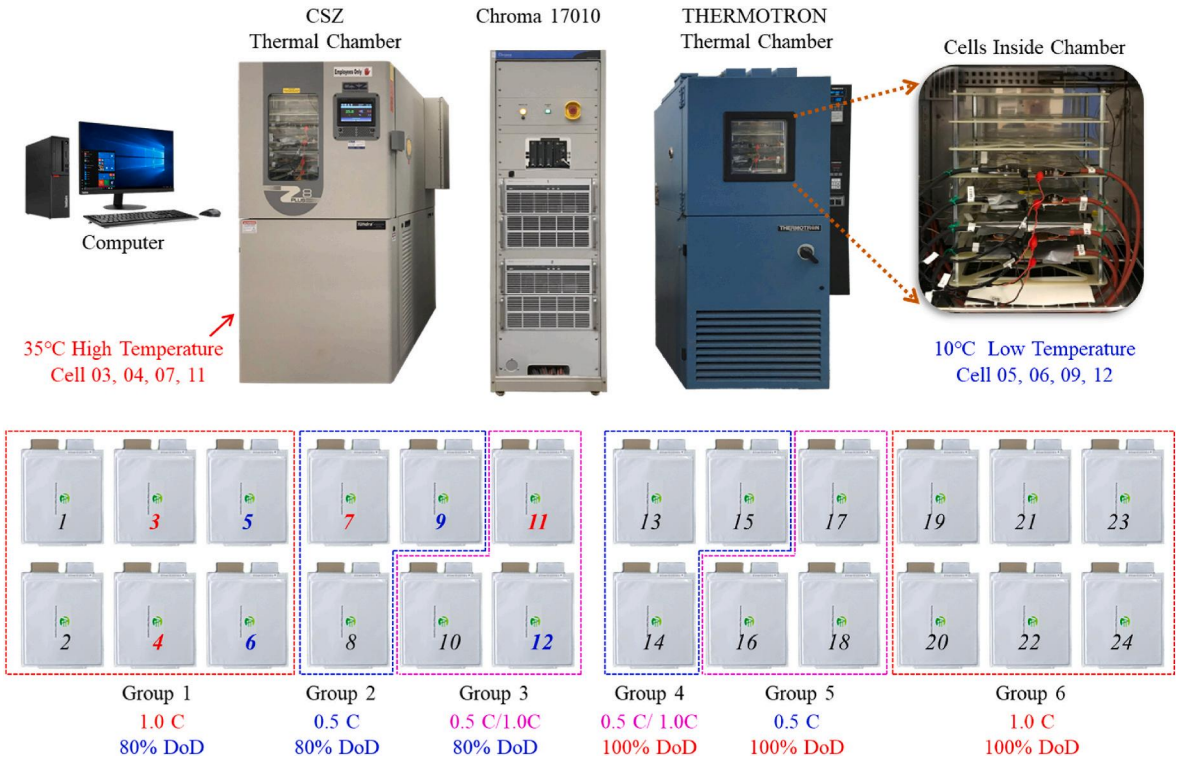

Fig. 1. Battery cell aging test system.

Table 2
The four stages of the battery cell aging test.

Group No.	Stage 1	Stage 2		Stage 3	Stage 4
	Initial Aging Test 1~240 cycles	Aging at different working conditions		Early Stage of Second Life	Late Stage of Second Life
	90 %–81% SOH 51Ah to 46Ah	To 600 cycles	To aging knee	75 %–60 % SOH 42Ah~34Ah	60 %–50 % SOH 34Ah~28Ah
Group1 Cell 01~06	100 % DoD 2.8V–4.2V 1C/1C (54A)	80 % DoD (3.0V–4.05V) 1C/1C (45A)		80 % DoD 3.0V–4.05V 0.3C/0.3C (12A)	67 % DoD 3.0V–4.05V 0.3C/0.3C (8A)
Group2 Cell 07~09		80 % DoD 0.5C/ 0.5C (22.5A)	80 % DoD 0.5C/ 0.5C		
Group3 Cell 10~12			80 % DoD 0.5C/ 1C		
Group4 Cell 13~15		100 % DoD 0.5C/ 0.5C	100 % DoD 0.5C/ 0.5C		
Group5 Cell 16~18			100 % DoD 0.5C/ 1C		
Group6 Cell 19~24		100 % DoD (2.8V–4.2V) 1C/1C (45A)			

capacity and impedance after the *N* aging cycles, which include a 0.2C capacity test, two 1C capacity tests, and a Hybrid Pulse Power Characterization (HPPC) test to calculate the battery impedance. The characteristic tests were conducted at 22 °C–25 °C room temperature. If the *N* aging cycles were conducted at 10 °C or 35 °C, the thermal chamber would be tuned to 22 °C and rest for 8 h before the characteristic test. The test conditions were not changed inside each test stage for consistent battery parameter evaluation, but they were changed between stages due to significantly degraded battery capacity and impedance. The 0.2C capacity is regarded as battery capacity. The HPPC test data was recorded at a 1-s time step for battery parameter calculation.

2.3.1. *Stage 1: 240 cycles initial aging test*

At the beginning of the aging process, all 24 batteries were cycled at the same test conditions to verify their performance consistency. In other words, we need to confirm that all the batteries degrade consistently under the same test conditions. Thus, the aging speed difference among the batteries in the later tests can be attributed to the working conditions instead of battery variance. The cycling current was 1C (54A) charging and discharging, 100 % depth of discharge (DoD), i.e., 2.8V–4.2V, and 22 °C–25 °C room temperature, as shown in Fig. 2(a). The battery surface temperature was about 32 °C, with a 10 °C temperature-rise.

The current of the 0.2C capacity test was 10.8A, and the voltage range of the four characteristics test cycles was 2.8V–4.2V.

2.3.2. *Stage 2: Battery aging test at different working conditions*

The 24 battery cells were divided into four groups after the first 240 aging cycles to test the battery aging at different DoD and current, as shown in Table 2. To distinguish the influence of 1C high current charging and discharging on the battery aging speed, they were further divided into six groups after 600 cycles. The 0.5C/1C means 0.5C charging and 1C discharging current. Because the batteries' capacity had already degraded to about 45Ah, 1C current was set to 45A, and 0.5C was set to 22.5A. The voltage range of 80 % DoD was set to 3.0V–4.05V, which was correspond to 3 %~85 % state of charge (SOC). The cycling was conducted at 22 °C–25 °C room temperature.

The high and low-temperature aging test started after 1080 cycles, as shown in Fig. 6. Cells 03, 04, 07, and 11 were moved to the 35 °C thermal chamber, while Cells 05, 06, 09, and 12 were moved to the 10 °C

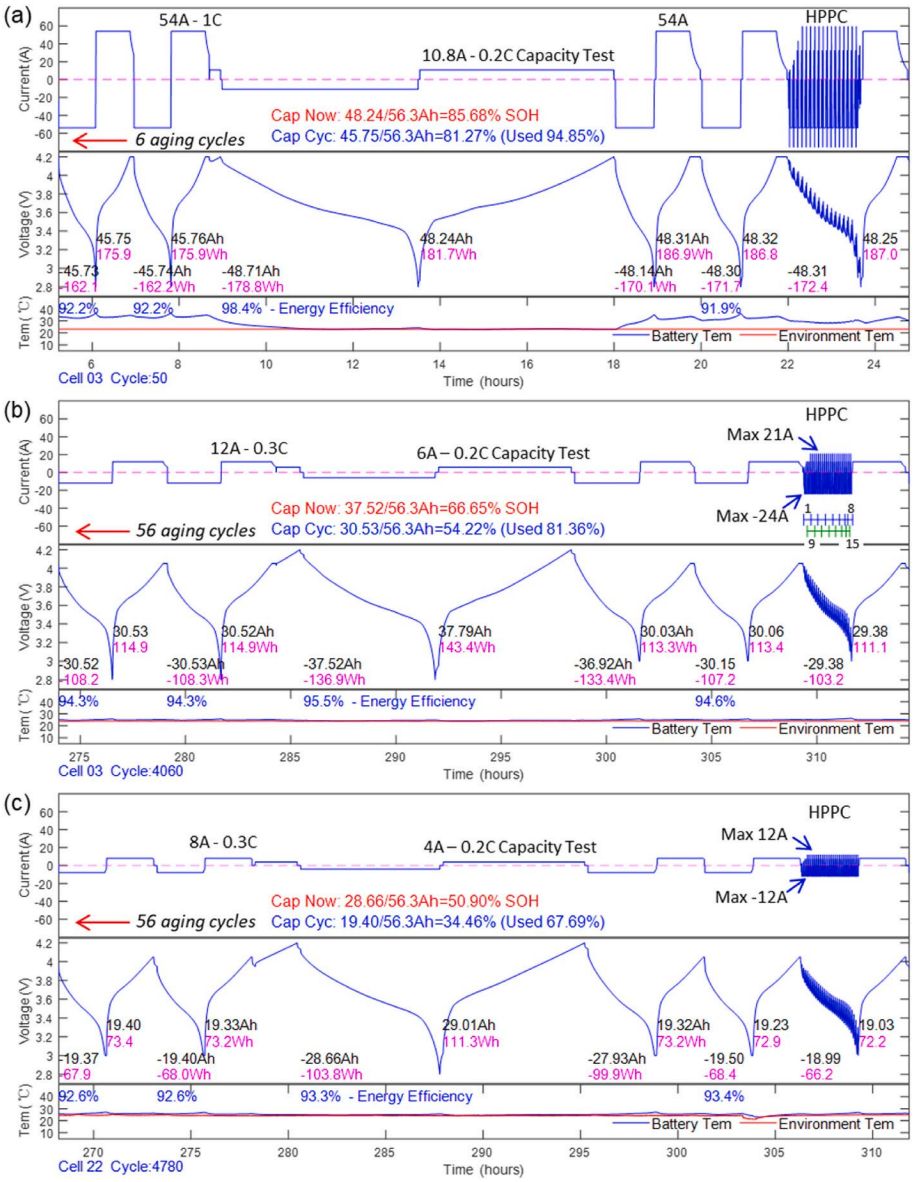

Fig. 2. Battery cell aging test data. (a) Stage 1: Initial aging test. Cell 03 after 50 cycles; (b) Stage 3: Early stage of second life. Cell 03 after 4060 cycles; (c) Stage 4: End of second life. Cell 22 after 4780 cycles.

thermal chamber, as shown in Fig. 1.

Some batteries, like Cells 04, 14, and 18, died directly in Stage 2 due to the fast degradation after the aging knee. Other batteries were transferred to improved working conditions at different stages of the aging knee to mimic second life operation, as listed in Table 3. The corresponding moments can also be found in the battery aging trajectories where the rapidly declining capacity curves leveled off.

Table 3
The time when the batteries were transferred to improved working conditions.

	SOH Range	Battery Cells	Second Life Value
Beginning of aging knee	78 %–75 %	09, 12, 21	>6000 cycles
Early stage of aging knee	75 %–60 %	02, 03, 07, 08, 11	2000~6000 cycles
Late stage of aging knee	60 %–50 %	05, 06, 13, 15, 16, 17, 19, 22, 23	0~2000 cycles
Unstable zone	50 %–45 %	01, 10	0
Died	<35 %	04, 14, 18, 20, 24	0

2.3.3. Stage 3: Early stage of second life – improved working conditions

The test conditions were improved to stop the aging knee. The DoD was set to 80 %, and the corresponding voltage was 3.0V–4.05V. The voltage range of Cells 03, 12, 13, and 22 was set to 2.8V–4.05V to see the impact of discharging to 0 % SOC. The current was reduced from 45A (1C) and 22.5A (0.5C) to 12A (0.3C), as shown in Fig. 2(b). The eight batteries cycled at high and low temperatures were still cycled under the specified temperatures to see the impact of temperature on the battery aging after the knee point.

The current of the 0.2C capacity test was reduced from 10.8A to 6A, and the voltage was still 2.8V–4.2V. The batteries' stability was poor after the knee point, and fully charging would induce fast degradation. Therefore, to avoid damage to the batteries, the two 1C capacity test cycles was changed to normal cycles with lower current and DoD. The current of the HPPC test cycle was also reduced to accommodate the significantly increased battery impedance.

2.3.4. Stage 4: Late stage of second life – further improved working conditions

The stabilities of the batteries further deteriorated after the SOH dropped below 60 % (34Ah). The cycling current was further reduced to 8A (0.25C–0.3C), and the voltage range was reduced to 3.0V–4.0V to maintain a slow and linear degradation, as shown in Fig. 2(c). The current of the 0.2C capacity test was reduced to 4A.

3. Battery impedance calculation

The battery capacity and impedance were tracked during the aging process. The discharging capacity at 0.2C is regarded as the battery capacity, and the HPPC test cycle is used to calculate the battery impedance. The 1-RC equivalent circuit model is used to simulate the battery dynamics [42,43]. The model consists of a voltage source, which is depicted by an open circuit voltage (OCV)-Ah curve, an ohmic resistance R_0, and an RC (diffusion resistance R_1 and capacitor C_1) network. Therefore, the battery impedance can be depicted with R_0 and R_1. The 1-RC model is:

$$\begin{cases} \dot{U}_1 = -\dfrac{1}{R_1 C_1} U_1 + \dfrac{1}{C_1} I_t \\ U_t = U_{OC} - U_1 - I_t R_0 \end{cases} \tag{1}$$

where U_1 is the voltage across the RC network, I_t is the current load of the battery, U_{OC} is the OCV, and U_t is the terminal voltage. Its discrete-time format can be written as:

$$\begin{cases} U_{1,k+1} = \exp(-\Delta t/R_1 C_1) \times U_{1,k} + [1 - \exp(-\Delta t/R_1 C_1)] \times I_{t,k} R_1 \\ U_t = U_{OC} - U_1 - I_t R_0 \\ D_1 = \exp(-\Delta t/R_1 C_1) \end{cases} \tag{2}$$

where k is the step, Δt is the time interval, which is 1 S in this study, $U_{1,k+1}$ is the value of U_1 at time step $k+1$, $I_{t,k}$ is the value of I_t at time step k, and D_1 is the time constant.

In this model, I_t is the input and U_t is the output, which are both measurable in the physical system. U_{OC}, R_0, R_1, and D_1 are the unknown model parameters. The particle swarm optimization (PSO) algorithm is used to calculate the battery parameters based on the HPPC test data. Due to the nonlinear nature of the battery parameters in the whole SOC range, the HPPC cycle is cut into 15 small pieces, as shown in Fig. 2(b), and the battery parameters are calculated on each data piece individually. The parameter vector under estimation for each data piece is:

$$\boldsymbol{X} = [U_{OC1}, U_{OC2}, R_0, R_1, D_1, U_{1,init}] \tag{3}$$

where U_{OC1} and U_{OC2} are the OCV on the two terminals of each data piece, and $U_{1,init}$ is the initial voltage of the RC network. After thousands of iterations, all the particles converge to one point, and the optimal parameter vector is identified. Then, the calculated battery parameters of the 15 data pieces are connected into parameter-Ah curves, as shown in Fig. 3(c)-(d). The values of R_0 and R_1 at about 75 % SOC, labeled as red triangular, are used to plot the battery aging trajectories in Figs. 6–8. The validation of data pieces 04 and 15 is illustrated in Fig. 3(a)–(b), where the model simulated voltage curves almost perfectly overlap with the measured voltage curves, proving the accuracy of the 1-RC model and parameters. The details of the algorithm were elaborated in Ref. [44]. Thus, it is not duplicated here.

4. Gas chromatography (GC) and morphology characterization

Nine of the 24 batteries died in the aging test, and four dead batteries swelled. Cell 04 and Cell 20 swelled during the battery cycling. However, Cell 14 and Cell 18 did not swell when they were dead, but swelled about one month after the batteries died, suggesting the decomposition of electrolyte continued after the test was finished. Fig. 4(b) shows two swelled batteries Cell 04, Cell 14, and a non-swelled dead battery Cell 19

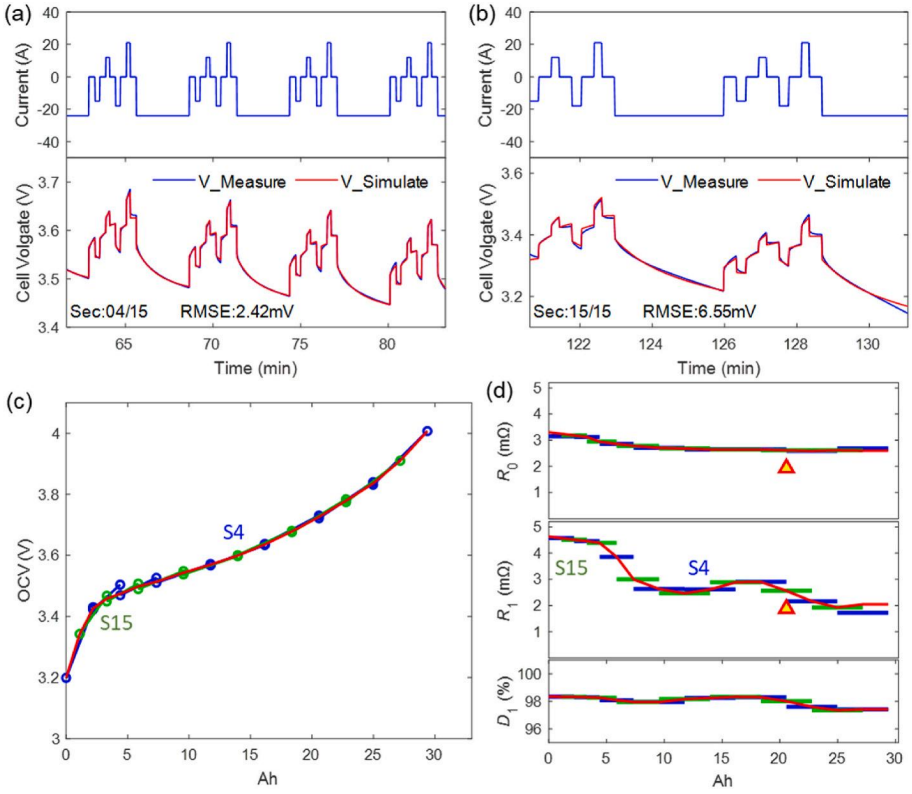

Fig. 3. The PSO-based battery parameter calculation for Cell 03 after 4060 aging cycles. (a) Validation of section 04; (b) Validation of section 15; (c) The connected OCV-Ah curve; (d) The battery impedance-Ah curves.

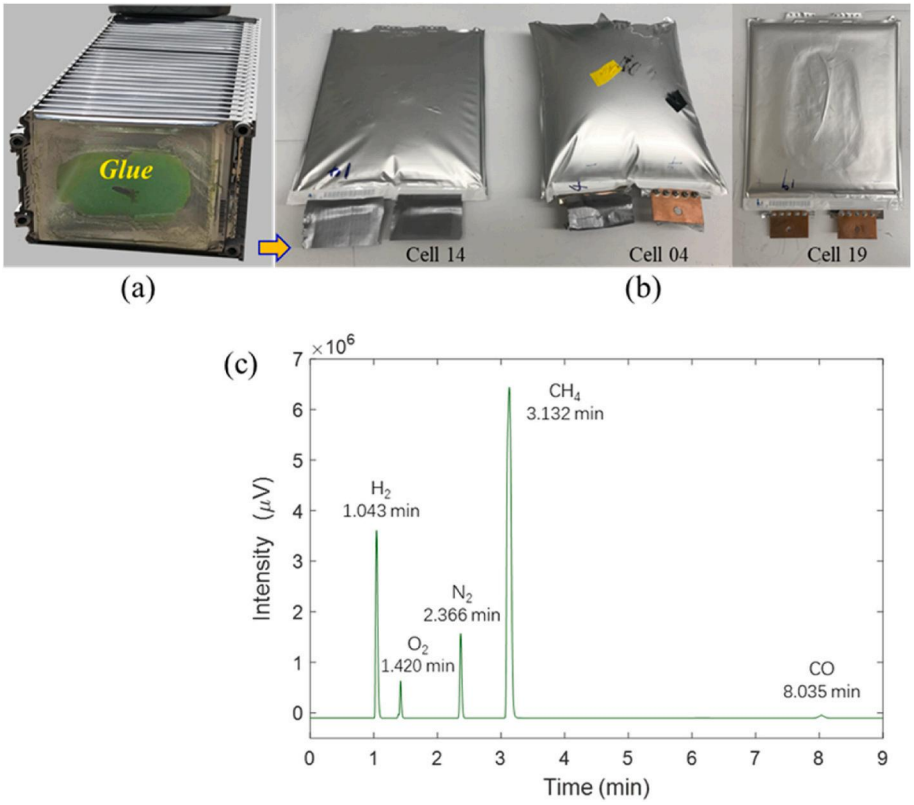

Fig. 4. (a) The 3P–9S battery module before the aging test; (b) The dead batteries; (c) GC analysis.

for comparison.

To study the gas composition of the swelled batteries, the gas of Cell 20 was collected using a syringe. GC was performed using a Shimadzu GC-2010 gas chromatograph equipped with a BID detector using helium as the carrier gas. The gas products were identified by comparing the observed retention times to those taken from the supplementary information of [45].

Fig. 4(c) shows the GC analysis result, where H_2, O_2, CH_4, and CO are detected. The concentrations were determined using the calibration curves from Ref. [45], which was developed using the same instrument under identical test conditions. The concentrations of H2, CO, and CH4 were determined to be 276140.5, 2225.0, and 94653.7 ppm, respectively. The presence of a large amount of H_2 indicates electrolyte decomposition occurred on the negative electrode [32].

The dead battery Cells 10, 20, and 24 were disassembled in a glove box protected by argon for material analysis. To investigate the material morphology on μm-level, a QUANTA FEG 450 scanning electron microscope (SEM) was used with an accelerating voltage of 20 kV. The SEM imaging was carried out in vacuum. Fig. 5 (a)-(b) show the positive electrode and negative electrode material of Cell 20. It is obvious that the negative electrode material structure already collapsed, and a large amount of graphite exfoliated. The positive electrode material looks undamaged. Fig. 5(c) presents the SEM image of the NMC positive electrode. The surface of the positive electrode seems unmodified and undamaged as no micro cracks or surface films are detected. Fig. 5(d) shows the SEM image of the graphite negative electrode. The single graphite particles of 10 μm size are clearly visible, but a large area of the graphite surface is covered by flocculent sludge, which is evidence of electrolyte decomposition on the negative electrode surface. These findings agree with the study in the literature [16]. Post-mortem study of the non-swelled battery Cell 10 and Cell 24 shows identical results as the swelled Cell 20.

Based on the above observations, all the evidence indicates that the battery aging knee is related to the large-scale failure of the negative

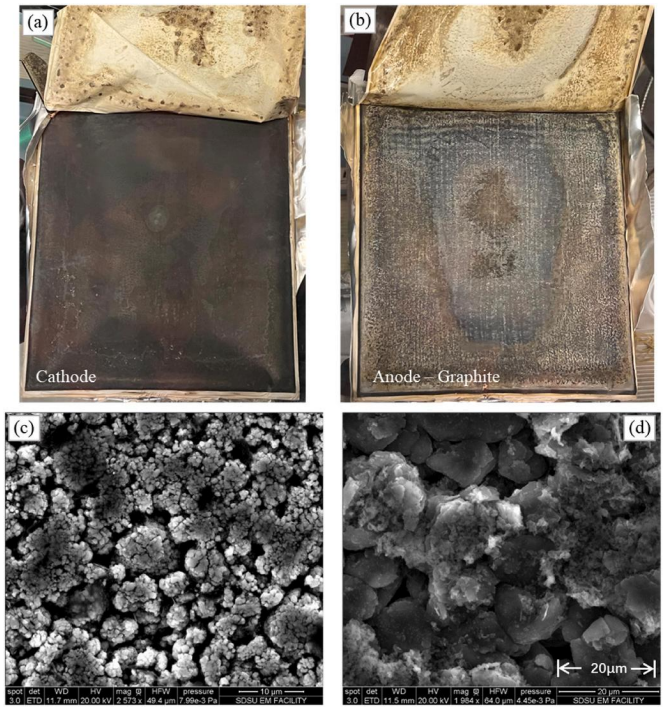

Fig. 5. Post-mortem analysis of Cell 20 (a) The positive electrode material; (b) The negative electrode graphite exfoliation; (c) SEM image of the NMC positive electrode; (d) SEM image of the graphite negative electrode.

electrode material. When fresh graphite and lithium were exposed to electrolyte after the negative electrode structure collapsed, violent side reactions would occur between the lithium and electrolyte without the

protection of SEI, consequently, resulting in aging knee and gas generation. Elevated temperature, high current and voltage would aggravate the side reactions.

5. Results and discussion

5.1. Battery aging before the knee point– first life operation

Fig. 6 presents the aging trajectories of the 24 battery cells before the aging knee. The initial characteristics test shows that the capacity of the 24 batteries was between 49.01Ah and 50.58Ah (87.1 %~89.8 % SOH), with a 2.8 % difference. R_0 was between 0.9 and 1.0 mΩ, and R_1 was between 1.0 and 1.1 mΩ. The batteries had a good consistency before the aging test.

5.1.1. Battery fast degradation and consistency evaluation in the initial 240 aging cycles

Fig. 6 shows that the batteries exhibited a fast capacity degradation in the first 240 aging cycles. The capacity degraded from approximately 50Ah to 46Ah (88.8 %~81.7 % SOH), and the capacity degradation rate is 29.6 % per 1000 cycles, or 1 % per 3.4 cycles, which is much higher than the normal value. The battery impedance R_0 and R_1 decreased about 10 % during this process. This is clear evidence that the SEI film or graphite particles on the negative electrode cracked because of the 1C-rate and 100 % DoD charging cycles.

The batteries were rested for months before the aging test, during which period, the SEI film on the graphite grew and lost porosity and activity. Thus, the impedance would increase about 10 %–20 %. When the batteries are back in use again, usually the impedance would decrease gradually to a normal level after dozens of charging cycles, and the porosity and activity of the SEI films are recovered. However, high current and fully charging during this process would impose too much stress on the SEI, combined with the 10 % volume change on the negative electrode during cycling, the SEI film could be damaged instead of activated. In this scenario, fresh graphite would be exposed to electrolyte, and the SEI film would reform on the negative electrode, which consumes a large amount of lithium-ion and graphite. This is the reason for the fast capacity degradation.

The SEI film rebuild process is similar to the "formation & aging" process in new battery manufacturing [13]. It requires a low current, e.g., 1/20 C-rate for the first charging, to form a stable SEI film. If the current is too large or the voltage is too high, violent side reactions would occur without the protection of stable SEI film, which would further induce negative electrode structure collapse, more side reactions, and fast capacity degradation.

Therefore, after a long time resting of LIBs, it is suggested to use the batteries mildly, e.g., use slow charging and charge to 80 %, for at least a couple of charging cycles to properly re-activate the battery material.

Despite the fast capacity degradation, the 24 batteries degrade uniformly in the first 240 aging cycles. As shown in Fig. 6., the capacity

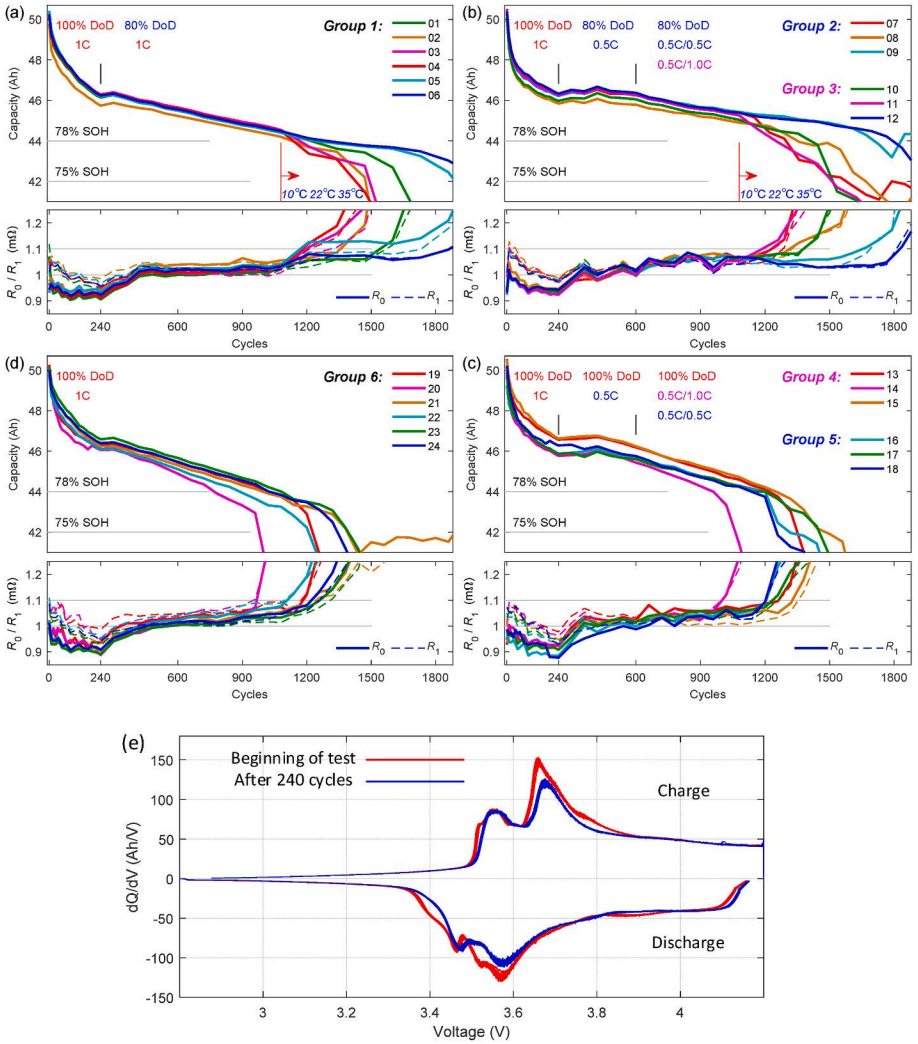

Fig. 6. (a)–(d) Battery first life aging trajectories. (e) dQ/dV analysis of 24 cells at the beginning and after 240 cycles.

degraded to 46.6Ah~45.8Ah (82.8 %~81.3 % SOH), with a 1.5 % difference. Furthermore, Fig. 6(e) compares the dQ/dV curves of the 24 batteries before and after the initial 240 test cycles. The curves of the 24 batteries are almost perfectly overlapped. These results together prove the consistency of the batteries, and they have consistent degradation behaviors during the initial 240 cycles.

5.1.2. Battery aging speed under different working conditions

The aging test was stopped for about three weeks after the initial 240 aging cycles for equipment maintenance. Fig. 6 shows that the fast degradation slowed down after the rest, and the impedance increased back to about 1mΩ and then stabilized. It suggests that reformed SEI film was built, and the battery aging was stabilized again.

Fig. 6 shows that the batteries degraded linearly in Stage 2 before the aging knee. The mean aging speed of the six groups from 600 to 1080 cycles is compared in Table 4, which is sorted from low to high. The "Aging/1000 cycles" is the capacity loss per 1000 cycles. Due to the variance in battery capacity and test DoD, it is also necessary to compare the battery aging speed with throughput ampere-hour. Therefore, "Aging/1000 E_Cycles" is compared in Table 4, where 50Ah throughput ampere-hour is regarded as one Equivalent Aging Cycle (E_Cycle). The result shows that although the aging speed difference among the six groups narrowed, the order remains unchanged. The aging speed of all batteries in Stage 2 is much lower than that in Stage 1 (29.6 %/1000 cycles).

5.1.3. The influence of DoD on battery aging speed

Table 4 and Fig. 6 show that all three groups of batteries cycled at 80 % DoD degrade slower than the batteries cycled at 100 % DoD. The aging speed can be reduced by approximately 2.2 % per 1000 cycles by reducing the charging cut-off voltage from 4.2V to 4.05V.

100 % DoD increases the risk of early aging knee. Cell 14 and Cell 20 entered the aging knee after 960 cycles, while other batteries cycled at 100 % DoD entered the aging knee between 1200 and 1300 cycles. Most batteries cycled at 80 % DoD (excluding the ones cycled at 35 °C) entered the aging knee between 1400 and 1500 cycles. This means the aging knee could be postponed by 200 cycles by reducing the charging cut-off voltage. Considering the aging test at different DoD started from 82 % SOH, the battery life improvement could be more significant if fully charging can be avoided from 100 % SOH.

5.1.4. The influence of C-rate on battery aging speed

The battery aging speed of Group 3 (0.5C/1C) and Group 1 (1C/1C) is 0.38 % and 0.70 % higher than that of Group 2 (0.5C/0.5C), respectively. The battery aging speed of Group 4 (0.5C/1C) and Group 6 (1C/1C) is 0.26 % and 0.53 % higher than that of Group 5 (0.5C/0.5C), respectively. This indicates both 1C high current charging and discharging would slightly increase the battery aging speed, and the impact is similar. Compared to the 2.2 % aging speed increase caused by 100 % DoD, the impact of 1C high current is much smaller.

In theory, high current charging is more likely to increase the battery aging speed than high current discharge because of the potential of lithium-ion plating. However, a similar impact indicates that the increased battery aging speed could be caused by other reasons, e.g., internal heat generation, instead of lithium-ion plating.

Table 4
Battery aging speed comparison of 600~1080 cycles.

	Group 2 Cell 08	Group 3 Cell 12	Group 1 Cell 06	Group 5 Cell 18	Group 4 Cell 13	Group 6 Cell 23
	0.5C/0.5C 80 % DoD	0.5C/1C 80 % DoD	1C/1C 80 % DoD	0.5C/0.5C 100 % DoD	0.5C/1C 100 % DoD	1C/1C 100 % DoD
Capacity Loss (%)	1.56 %	1.74 %	1.90 %	2.69 %	2.81 %	2.94 %
Aging/1000 cycles	3.25 %	3.63 %	3.95 %	5.59 %	5.85 %	6.12 %
Aging/1000 E_Cycles	4.42 %	4.91 %	5.41 %	6.51 %	6.78 %	7.11 %

5.1.5. The influence of temperature on battery aging speed

Cells 03, 04, 07, and 11 were moved to the 35 °C thermal chamber after 1080 aging cycles. Fig. 6 shows that the aging speed of all four batteries increased instantly after that point. For example, the aging speed of Cell 11 increased to 13.9 % per 1000 cycles between 1080 and 1500 aging cycles, which is much higher than the previous value of 3.63 %.

Cells 05, 06, 09, and 12 were moved to the 10 °C thermal chamber after 1080 aging cycles. Fig. 6 shows that all four batteries reached the aging knee at about 1800 aging cycles, which means they survived 300 to 400 more cycles before the aging knee. The impedance of Cell 05 and Cell 06 increased by 10 %–15 %. However, the impedance of Cell 09 and Cell 12 (with 0.5C charging current) did not increase.

Therefore, the conclusion is that 15 °C–25 °C is ideal for battery operation. 10 °C low temperature would help improve battery life compared to 20 °C. However, the charging current has to be limited, e.g., below 0.3C, to avoid internal resistance increase and achieve a higher energy efficiency. This means the batteries of EVs and BESSs operating in cold climate areas only need to be heated up to 10 °C instead of 20 °C for slow charging, thus saving the cost of heating the batteries. However, if fast charging is applied, it is better to heat up the batteries to 15 °C to avoid lithium plating. The optimal temperature of the Nissan Leaf Gen 3 battery can be extended to 10 °C–25 °C with conditions.

5.1.6. Detection of aging knee

Fig. 6 shows that all the batteries tend to reach the aging knee when the capacity degraded to 44Ah~42Ah (78 %~75 % SOH), regardless of the working conditions and aging cycles.

The battery impedance barely increased before the aging knee. It only increased by about 5 % compared to a new battery, which can be hardly detected because it is within the noise range. However, the impedance started to increase quickly after the knee point. If the impedance is detected 50 % higher than the normal value, then it is very confident to declare that the battery entered the aging knee.

The BMS usually has built-in algorithms to detect the battery pack capacity and battery cell impedance. For example, the capacity can be evaluated with a deep discharge and fully charging process. The battery impedance can be calculated online using Extended Kalman Filter (EKF) or Recursive Least Squares (RLS) algorithm. Therefore, the battery capacity and impedance can be used as indicators to detect the aging knee. When the battery capacity degrades to 80 % or impedance increases by 20 %, the BMS should give a warning of the high risk of the occurrence of the aging knee. Then, some measures must be taken, e.g., only allowed to charge to 80 % SOC and reduce the DC charging current, to prolong the battery life. When the battery capacity degrades to 75 % and impedance increases by 50 %, which shows clear evidence of aging knee, the battery pack is unsuitable for vehicle use and should be repurposed right away to maximize its second life value.

5.1.7. The proposed strategies to extend the life of Nissan Leaf e + batteries

According to the aging test analysis, fully charging, 1C high current, and 35 °C high temperature would accelerate battery degradation. Fully charging brings more damage to the battery life compared to 1C high current. If two or three factors occur simultaneously, it will further accelerate battery aging and induce early aging knee. Hence, the following recommendations are suggested for operating the Nissan Leaf e+.

First, drivers should be given the option to set the charging cut-off SOC, just like Tesla does, and the default value should be set to 80 %. Drivers need to be educated that fully charging the battery would reduce battery life, while deep discharge to 0 % SOC would not. Some people

still believe that the battery should stay in a fully charged state and should not be fully discharged. This is the rule applicable to lead-acid batteries but not to LIBs. Some taxi drivers would like to charge the battery to 100 % twice a day using fast charging [41,46], which is stressing the batteries. If the working SOC window can be moved down from 50 %~100 %–30 %~80 %, the battery degradation could be much slower, and the risk of battery swelling would also decrease.

Secondly, slow charging should be used as much as possible instead of fast charging.

Thirdly, park the car in a cool area to avoid high temperatures. Elevated temperatures and a fully charging can not only accelerate battery degradation while driving, but also increase calendar aging while resting [30,47]. When the temperature is high, the BMS should limit the charging current and charging cut-off voltage. A liquid cooling system is a better solution for the next generation of Nissan battery pack design to avoid high temperatures.

Fourthly, when the BMS detects that the battery capacity has degraded to 80 %, or impedance increased by 20 %, some limitations should be applied to extend battery life. For example, prohibit fast charging, and limit the charging voltage to 4.05V or 80 % SOC.

Finally, the battery pack shall be replaced when its capacity drops to 75 % and impedance increases by 50 %. This is the best time to repurpose the battery pack to maximize both its first and second life value.

The real-world EV battery aging speed is believed to be about 12 % per 1000 cycles. For example, Tesla declared that the mean battery degradation is about 12 % after 200,000 miles [48]. Assuming the driving distance is 200 miles per charge, 200,000 miles equals 1000 cycles. The EV battery aging speed is much higher than the 3.15 % ~6.12 % battery aging speed in Table 4. That is because fully charging, high current, high temperature, and calendar aging cannot be totally avoided in real-life operations. In other words, if the driver takes good care of the car, the battery degradation speed could be reduced by half, thus doubling the battery life.

5.2. Battery aging test after the knee point – second life operation

To study the aging performance of the EV batteries after the aging knee and explore the second life potential, we tried to improve the operating conditions to stop the aging knee and extend the battery life. Different DoD and current configurations were tested on Cell 20 and Cell 19 after the knee point, and finally, we found that if the current is reduced to 12A (<0.4C) and the voltage is between 3.0V and 4.05V (80 % DoD), the aging knee can be stopped. Then, some of the batteries were transferred to the improved test conditions at different stages of the aging knee, which is listed in Table 3. Fig. 7 shows the battery aging trajectories after the aging knee was stopped. The test conditions are described in Section 2.3.3, and the test data is illustrated in Fig. 2(b).

When the battery capacity dropped to below 34Ah (60 % SOH), its material stability further deteriorated. The cycling current was further reduced to 8A, and the voltage range was reduced to 3.0V–4.0V (70 % DoD) to accommodate further reduced capacity and maintain a stable degradation. The test conditions are described in Section 2.3.4, and the test data is illustrated in Fig. 2(c).

Therefore, the 75 %~60 % SOH is defined as the early stage of second life of the EV batteries, while the 60 %~50 % SOH is defined as the late stage of second life. The second life window is labeled with colored backgrounds in Fig. 7. Although Cell 01 and Cell 10 survived 3000 and 2000 aging cycles below 50 % SOH, respectively, they are not useable due to very low cyclable capacity, high impedance, low current, and low energy efficiency.

5.2.1. The battery aging speed in the second-life window

Table 5 shows the battery aging speed in the second-life window. Cell 03 and Cell 08 represent the early stages of their second life. The aging speed is about 2.08 %–3.18 % per 1000 cycles. Cell 15 and Cell 23 represent the late stage of second life. The aging speed is 3.75 % and 4.64 %, respectively. The result shows that the battery aging speed is as low as the first life before the aging knee. The aging speed with E_Cycle is between 3.4 % and 10.41 %, where 50Ah throughput ampere-hour is regarded as one E_Cycle. The aging speed is also at a low level.

The test proves that the battery aging knee can be stopped at any stage after the knee point, as long as the capacity is above 50 % nominal.

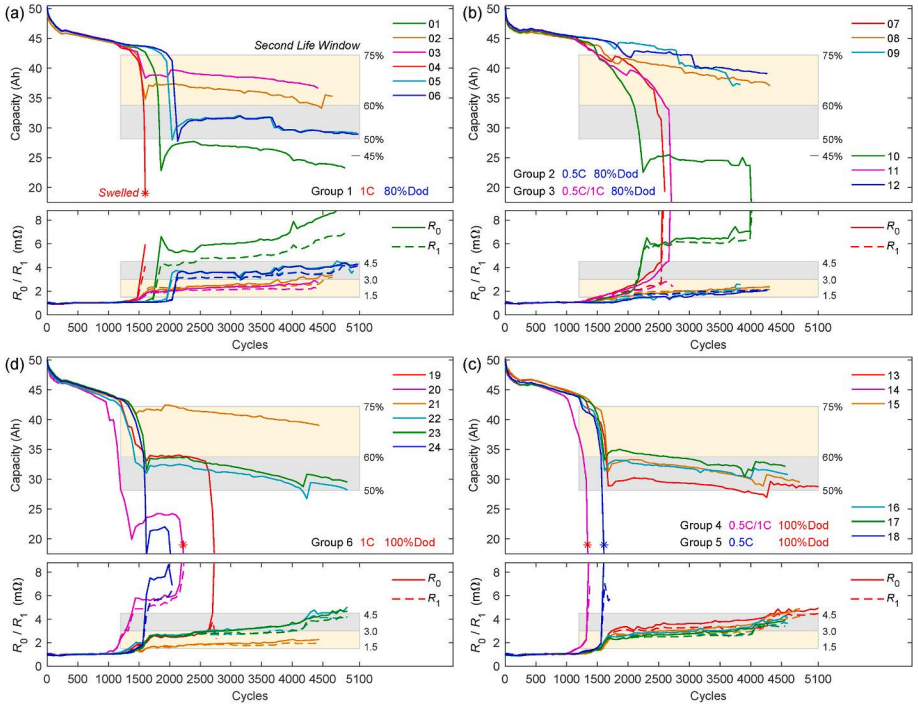

Fig. 7. Battery aging trajectories after the knee point (* sign indicates the swelled dead batteries).

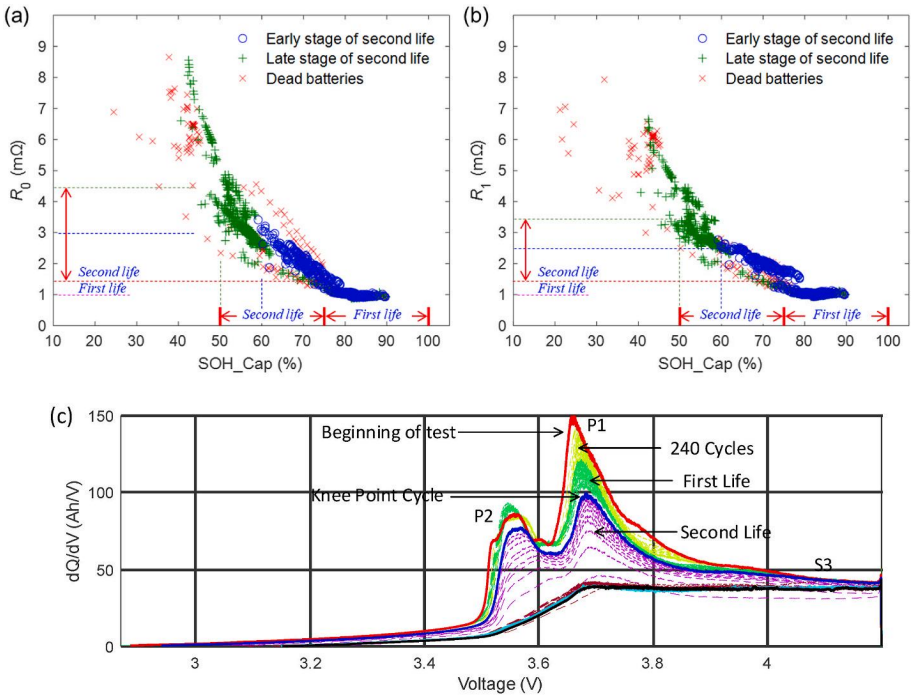

Fig. 8. Battery impedance increase and dQ/dV analysis; (a) R_0 increase with capacity degradation; (b) R_1 increase with capacity degradation; (c) dQ/dV analysis of Cell 10.

Table 5
Battery aging speed of second life.

	Cell 03 Early Stage	Cell 08 Early Stage	Cell 11 35 °C	Cell 15 Late Stage	Cell 23 Late Stage
Cycle Range	2080–4360	2090–4250	1171–2606	2280–3840	2280–4180
Capacity Loss (%)	4.73 %	6.87 %	19.27 %	7.20 %	8.82 %
Aging/1000 cycles	2.08 %	3.18 %	13.43 %	3.75 %	4.64 %
Aging/1000 E_Cycles	3.40 %	5.06 %	21.14 %	8.35 %	10.41 %

5.2.2. *Second life evaluation of the Nissan Leaf Gen 3 batteries*

If the battery pack is repurposed at 75 % SOH, then the second life window is 75 %~50 % SOH. The mean battery aging speed is about 4 % per 1000 cycles according to Table 5. Therefore, the estimated second life is at least 6000 cycles. If the battery pack is charged once a day, the service time can reach 16 years. Table 6 compares the battery performance at different aging states. The battery pack's maximum power is reduced from 160 kW to 15 kW and 9.6 kW after it is repurposed for BESS.

Table 6
Nissan Leaf Gen 3 battery pack performance at different aging states.

	First Life - EV	Second Life – Early Stage	Second Life – Late Stage
SOH (%)	100 % ~ 75 %	75 % ~ 60 %	60 % ~ 50 %
Energy Capacity (kWh)/	59–44 kWh	44–35 kWh	35–29 kWh
Pack Energy Density (Wh/kg)	143.9–107.9	107.9–86.3	86.3–72.0
Current (A)/Power (kW)/C-rate	400A/160kW/ 2.7C	36A/15kW/0.3C	24A/9.6kW/ 0.25C
Energy Efficiency at 0.2C (%)	>98 %	98 %–95 %	95 %–93 %
Aging Cycles	1500–2500	4000	2000
Service Time (year)	10–15 years	11 years	5 years
Impedance R_0 (mΩ)	1mΩ	1.5–3.0 mΩ	3.0–4.5 mΩ
Aging/1000 cycles	6 %–12 %	4 %	5 %
Aging/1000 E_cycles (50Ah)	6 %–12 %	5 %	10 %
Aging/year	1.5 % ~ 2.5 %	1.5 %	2.0 %

The batteries have a superior performance in the first 4000 cycles of second life before the SOH drops to 60 %, equivalent to 11 years of operation. Afterward, the power, energy efficiency, and stability of the batteries started to worsen. For example, the 0.2C energy efficiency decreased from 95 % to 93 %, as shown in Fig. 2(b)–(c). Nevertheless, the battery is still useable until 50 % SOH with well-controlled working conditions.

5.2.3. *The impact of working conditions on the second life*

Although the battery aging knee can be stopped or avoided by improving the working conditions, the batteries are very unstable after the knee point (75 % SOH). If the working conditions are not well controlled, the battery could die quickly.

High temperature would significantly shorten the second life. Fig. 7 shows that Cell 07 and Cell 11 were switched to improved working conditions but still in the 35 °C environment. The aging speed of the two batteries was about 13 %–14 % per 1000 cycles, and they only survived 700 s-life cycles before dying. For comparison, Cell 08 working at 22 °C–25 °C survived more than 2000 cycles, and it is still working now.

A low temperature of 10 °C could also induce fast degradation for aged LIBs. For example, Cell 05 and Cell 06 experienced a capacity drop at 3600 aging cycles. While Cell 09 and Cell 12 experienced a capacity drop between 2700 and 3000 aging cycles. By reducing the charging current from 12A to 6A and 8A, respectively, the fast degradation can be avoided. Therefore, the solution is either to heat up the battery to 15 °C–20 °C or maintain a 10 °C low temperature while reducing the

current and charging cut-off voltage to prevent fast degradation.

Charging to a higher voltage could also kill the battery instantly. The charging voltage of Cell 19 was intentionally increased from 4.05V to 4.15V at 2700 aging cycles. Then, it died in the following 20 cycles. For comparison, Cell 22 and Cell 23 survived a much longer second life.

It should be noted that deep discharge to 2.8V low cut-off voltage (not over-discharge) did not hurt the batteries. Cells 03, 12, 13, and 22 were all cycled between 2.8V and 4.05V, and no fast degradation occurred.

5.2.4. The strategies to extend battery second life

First, the operational voltage range should be set to 3.0V–4.05V (80 % DoD). When the SOH drops below 60 %, the voltage range should be further reduced to 3.0V–4.0V (70 % DoD).

Secondly, the battery temperature should be strictly controlled below 30 °C, and 15 °C–25 °C is preferable. The battery can work at 10 °C low temperature, however, the current and charging voltage should be further reduced to prevent lithium plating.

Thirdly, the optimal current is 0.2C or below, and the peak current should be no more than 0.3C.

Fourthly, the batteries should operate every day to maintain their material activity. Long-time resting (months) of the batteries should be avoided to mitigate the loss of material activity and calendar aging. Additionally, managing the SoC and storage conditions during prolonged periods of non-use can also mitigate the effects of calendar aging.

5.3. Battery impedance and dQ/dV analysis

Figs. 6 and 7 show that the impedance of the batteries did not have noticeable change until 80 % SOH. Then, the battery impedance increased linearly with battery capacity degradation. In order to draw a clear relationship between the battery impedance and capacity, Fig. 8 (a) and (b) plots the R_0-SOH and R_1-SOH relationships. The blue dots represent the batteries in the early stage of second life. The green dots represent the batteries in the late stage of second life. The red dots represent the dead batteries.

The values of R_0 and R_1 did not change obviously between 90 % and 80 % SOH. However, R_0 and R_1 (blue and green) show a clear linear relationship with SOH in the 75 %–50 % second life window. Therefore, both capacity and impedance can be used to evaluate the state of batteries during their second life. The red dots are scattered out of the mainstream, indicating a violent battery characteristic change during the aging knee.

Incremental capacity analysis (ICA) can be used to identify battery degradation modes [49,50]. Fig. 8(c) shows the dQ/dV curves of Cell 10. Two peaks (P1 and P2) and one shoulder area (S3) are observed in the ICA curves. Intensity variation and position shift of these features are correlated with mixed degradation modes: the Loss of Lithium Inventory (LLI), the loss of active material (LAM) at the negative electrode, and LAM at the positive electrode [51].

The position of P1 shifts to the higher voltage and its intensity decreases monotonously during the whole aging process. LLI induces capacity loss at the early stages. The decrease in S3 intensity indicates the LAM at the positive electrode. Initially, the subtle change in P2 indicates LAM at the positive electrode, alongside LLI. After the aging knee, P2 decreases significantly and shifts rapidly to high voltages, eventually disappearing. This implies that the major battery degradation mechanism after the aging knee shifts to LLI and LAM at the negative electrode [14]. This agrees with the post-mortem analysis, which shows a large amount of graphite exfoliated from the negative electrode.

5.4. Gas generation

5.4.1. The causes of gas generation

Only four of the nine dead batteries swelled. It is very important to study what working conditions would induce battery swelling, and why other batteries did not swell. Three factors can induce battery swelling, i.e., fully charging, 1C fast charging, and elevated temperatures. All the nine dead batteries are compared in Table 7. The "Violent Aging" in the table means the battery experienced continuous aging knee until it was dead. On the contrary, other batteries experienced slow degradation or switched to improved working conditions.

Table 7 shows that all four swelled batteries encountered two or three trigger factors, while most not-swelled batteries only encountered one or no trigger factors. Cell 24 did not swell because it was disassembled right away after it died for material analysis. In other words, Cell 24 might also swell one month after death if it was not disassembled.

Obviously, the more trigger factors encountered, the more risk of battery gas generation and swelling. One factor alone would not induce gas generation. In other words, if the four trigger factors can be removed, the battery gas generation and swelling could be avoided.

5.4.2. The safety risk of gas generation

As discussed in Section 5.2.4, the suggested SLB working conditions include: 3.0V–4.05V (80 % DoD) voltage, 0.2C–0.3C current rate, and 15 °C–25 °C temperature. Obviously, the first three trigger factors for gas generation are totally ruled out. In this condition, violent aging would also not happen. Therefore, we are confident that the risk of gas generation and swelling during the second life application of Nissan Leaf Gen 3 batteries is almost zero if the recommendations proposed in this paper are followed.

For the first life operations in EVs, the gas generation of the batteries can also be avoided by charging to 80 % SOC, using slow charging, and keeping the car in a cool environment. If some factor cannot be avoided, the driver should try to avoid two or more trigger factors occurring simultaneously. For example, if elevated temperature cannot be avoided, then only use slow charging, and charge to 80 % SOC.

6. Conclusions

This paper conducted a comprehensive aging study on Nissan Leaf Gen 3 batteries, aiming to develop solutions to address the aging knee and gas generation issues and evaluate their second-life potential and safety risks. The key findings of this study include:

1. The battery aging knee can be prevented or stopped by improving the working conditions. The recommended strategies include: 3.0V–4.05V voltage range (80 % DoD), 0.2C–0.3C current, and 15 °C–25 °C temperature. The battery aging speed can be reduced to 4 % per 1000 cycles.
2. The batteries tend to reach the aging knee when the capacity drops to 78 %~75 %. Their second life window is 75 %~50 % SOH. The estimated second life is 4000–6000 cycles or 11–16 years if the working conditions of the batteries can be well controlled.
3. The optimal time to retire and repurpose the battery pack from the EV is when the capacity drops to 75 % and the impedance increases by 50 %.

The impact of different working conditions on the battery aging was studied. The result shows that fully charging the batteries would induce fast degradation and early aging knee, while deep discharge to 0 % SOC imposes no harm to the batteries. Both 1C charging and discharge would accelerate battery aging. An elevated temperature of 35 °C would induce fast degradation, but a 10 °C low temperature can extend the battery life.

Based on the analysis, recommendations are proposed to the EV drivers to extend battery life which include: avoiding fully charging if not necessary (charge to 80 % SOC); using slow charging as much as possible; and parking the vehicle in a cool environment. It is also suggested that the EV manufacturer shall give the driver the option to set the charging cut-off SOC, and liquid cooling is recommended.

The battery swelling issue was studied. Gas generation can only be

Table 7
Battery swelling comparison.

	Cell 04	Cell 14	Cell 20	Cell 18	Cell 07	Cell 10	Cell 11	Cell 19	Cell 24
Fully Charging		○	○	○		○			○
1C Charging	○		○						
35 °C	○				○		○		
Violent Aging	○	○	○	○					○
Swelled	○○○	○○	○○	○					

triggered by multiple factors working together. If the second life utilization follows the proposed strategies listed above, all four trigger factors can be ruled out. Thus, the risk of battery swelling can be eliminated.

Post-mortem analysis on three dead batteries shows large-scale graphite exfoliation on the negative electrode. GC analysis and SEM image also indicate negative electrode material failure, while the NMC positive electrode material is in good condition. Therefore, the battery aging knee and gas generation are both related to the negative electrode failure.

In summary, this study clarified the prospect of the second life utilization of LIBs with aging knee issues, and proposed strategies to ensure the long second life. The safety concerns regarding gas generation can also be eliminated. It provides valuable recommendations for both the first life and second life operation of EV batteries.

CRediT authorship contribution statement

Wei Gao: Writing – original draft, Methodology, Investigation, Formal analysis, Data curation, Conceptualization. **Zhi Cao:** Writing – original draft. **Yuhong Fu:** Investigation, Data curation. **Christopher Turchiano:** Writing – review & editing, Investigation. **Naser Vosoughi Kurdkandi:** Investigation. **Jing Gu:** Investigation. **Chirs Mi:** Writing – review & editing, Supervision, Funding acquisition.

Declaration of competing interest

The authors declare the following financial interests/personal relationships which may be considered as potential competing interests.

Chris Mi reports financial support was provided by California Energy Commission. If there are other authors, they declare that they have no known competing financial interests or personal relationships that could have appeared to influence the work reported in this paper.

Data availability

The authors do not have permission to share data.

Acknowledgment

The authors would like to acknowledge the financial support of the California Energy Commission under grant number EPC-19-053.

References

[1] N. King, EVs forecast to account for two thirds of global light-vehicle sales in 2035. https://www.ev-volumes.com/, 2024.
[2] X. Hu, X. Deng, F. Wang, Z. Deng, X. Lin, R. Teodorescu, et al., A review of second-life lithium-ion batteries for stationary energy storage applications, Proc. IEEE 110 (2022) 735–753, https://doi.org/10.1109/jproc.2022.3175614.
[3] W. Gao, Z. Cao, N.V. Kurdkandi, Y. Fu, C. Mi, Evaluation of the second-life potential of the first-generation Nissan Leaf battery packs in energy storage systems, eTransportation (2024), https://doi.org/10.1016/j.etran.2024.100313.
[4] X.-G. Yang, Y. Leng, G. Zhang, S. Ge, C.-Y. Wang, Modeling of lithium plating induced aging of lithium-ion batteries: transition from linear to nonlinear aging, J. Power Sources 360 (2017) 28–40, https://doi.org/10.1016/j.jpowsour.2017.05.110.
[5] E. Hossain, D. Murtaugh, J. Mody, H.M.R. Faruque, M.S. Haque Sunny, N. Mohammad, A comprehensive review on second-life batteries: current state, manufacturing considerations, applications, impacts, barriers & potential solutions, business strategies, and policies, IEEE Access 7 (2019) 73215–73252, https://doi.org/10.1109/access.2019.2917859.
[6] Y. Hua, X. Liu, S. Zhou, Y. Huang, H. Ling, S. Yang, Toward sustainable reuse of retired lithium-ion batteries from electric vehicles, Resour. Conserv. Recycl. 168 (2021), https://doi.org/10.1016/j.resconrec.2020.105249.
[7] M. Shahjalal, P.K. Roy, T. Shams, A. Fly, J.I. Chowdhury, M.R. Ahmed, et al., A review on second-life of Li-ion batteries: prospects, challenges, and issues, Energy 241 (2022), https://doi.org/10.1016/j.energy.2021.122881.
[8] W. Li, E.M. Erickson, A. Manthiram, High-nickel layered oxide cathodes for lithium-based automotive batteries, Nat. Energy 5 (2020) 26–34, https://doi.org/10.1038/s41560-019-0513-0.
[9] A. Manthiram, B. Song, W. Li, A perspective on nickel-rich layered oxide cathodes for lithium-ion batteries, Energy Storage Mater. 6 (2017) 125–139, https://doi.org/10.1016/j.ensm.2016.10.007.
[10] S. Zhang, P. Gao, Y. Wang, J. Li, Y. Zhu, Cobalt-free concentration-gradient Li[Ni0.9Mn0.1]O2 cathode material for lithium-ion batteries, J. Alloys Compd. 885 (2021), https://doi.org/10.1016/j.jallcom.2021.161005.
[11] X. Shen, Z. Tian, R. Fan, L. Shao, D. Zhang, G. Cao, et al., Research progress on silicon/carbon composite anode materials for lithium-ion battery, J. Energy Chem. 27 (2018) 1067–1090, https://doi.org/10.1016/j.jechem.2017.12.012.
[12] H. Shen, H. Wang, M. Li, C. Li, Y. Zhang, Y. Li, et al., Thermal runaway characteristics and gas composition analysis of lithium-ion batteries with different LFP and NCM cathode materials under inert atmosphere, Electronics 12 (2023), https://doi.org/10.3390/electronics12071603.
[13] X. Han, L. Lu, Y. Zheng, X. Feng, Z. Li, J. Li, et al., A review on the key issues of the lithium ion battery degradation among the whole life cycle, eTransportation 1 (2019), https://doi.org/10.1016/j.etran.2019.100005.
[14] P.M. Attia, A. Bills, F. Brosa Planella, P. Dechent, G. dos Reis, M. Dubarry, et al., Review—"Knees" in lithium-ion battery aging trajectories, J. Electrochem. Soc. 169 (2022), https://doi.org/10.1149/1945-7111/ac6d13.
[15] H. You, J. Zhu, X. Wang, B. Jiang, X. Wei, H. Dai, Nonlinear aging knee-point prediction for lithium-ion batteries faced with different application scenarios, eTransportation 18 (2023), https://doi.org/10.1016/j.etran.2023.100270.
[16] S.F. Schuster, T. Bach, E. Fleder, J. Müller, M. Brand, G. Sextl, et al., Nonlinear aging characteristics of lithium-ion cells under different operational conditions, J. Energy Storage 1 (2015) 44–53, https://doi.org/10.1016/j.est.2015.05.003.
[17] J.C. Burns, A. Kassam, N.N. Sinha, L.E. Downie, L. Solnickova, B.M. Way, et al., Predicting and extending the lifetime of Li-ion batteries, J. Electrochem. Soc. 160 (2013) A1451–A1456, https://doi.org/10.1149/2.060309jes.
[18] Y. Leng, S. Ge, D. Marple, X.-G. Yang, C. Bauer, P. Lamp, et al., Electrochemical cycle-life characterization of high energy lithium-ion cells with thick Li(Ni0.6Mn0.2Co0.2)O2and graphite electrodes, J. Electrochem. Soc. 164 (2017) A1037–A1049, https://doi.org/10.1149/2.0451706jes.
[19] M. Klett, R. Eriksson, J. Groot, P. Svens, K. Ciosek Högström, R.W. Lindström, et al., Non-uniform aging of cycled commercial LiFePO4//graphite cylindrical cells revealed by post-mortem analysis, J. Power Sources 257 (2014) 126–137, https://doi.org/10.1016/j.jpowsour.2014.01.105.
[20] L. Yang, X. Cheng, Y. Gao, Y. Ma, P. Zuo, C. Du, et al., Lithium deposition on graphite anode during long-term cycles and the effect on capacity loss, RSC Adv. 4 (2014) 26335–26341, https://doi.org/10.1039/c4ra02096k.
[21] M. Dubarry, C. Truchot, M. Cugnet, B.Y. Liaw, K. Gering, S. Sazhin, et al., Evaluation of commercial lithium-ion cells based on composite positive electrode for plug-in hybrid electric vehicle applications. Part I: initial characterizations, J. Power Sources 196 (2011) 10328–10335, https://doi.org/10.1016/j.jpowsour.2011.08.077.
[22] M. Broussely, P. Biensan, F. Bonhomme, P. Blanchard, S. Herreyre, K. Nechev, et al., Main aging mechanisms in Li ion batteries, J. Power Sources 146 (2005) 90–96, https://doi.org/10.1016/j.jpowsour.2005.03.172.
[23] S. Atalay, M. Sheikh, A. Mariani, Y. Merla, E. Bower, W.D. Widanage, Theory of battery ageing in a lithium-ion battery: capacity fade, nonlinear ageing and lifetime prediction, J. Power Sources 478 (2020), https://doi.org/10.1016/j.jpowsour.2020.229026.
[24] M. Haris, M.N. Hasan, S. Qin, Degradation curve prediction of lithium-ion batteries based on knee point detection algorithm and convolutional neural network, IEEE Trans. Instrum. Meas. 71 (2022) 1–10, https://doi.org/10.1109/tim.2022.3181307.
[25] K. Liu, X. Tang, R. Teodorescu, F. Gao, J. Meng, Future ageing trajectory prediction for lithium-ion battery considering the knee point effect, IEEE Trans. Energy Convers. 37 (2022) 1282–1291, https://doi.org/10.1109/tec.2021.3130600.
[26] S. Sohn, H.-E. Byun, J.H. Lee, Two-stage deep learning for online prediction of knee-point in Li-ion battery capacity degradation, Appl. Energy 328 (2022), https://doi.org/10.1016/j.apenergy.2022.120204.

[27] X. Jia, C. Zhang, Y. Li, C. Zou, L.Y. Wang, X. Cai, Knee-point-conscious battery aging trajectory prediction based on physics-guided machine learning, IEEE Trans. Transp. Electrification (2023) 1, https://doi.org/10.1109/tte.2023.3266386, 1.
[28] Y. Ke, Y. Jiang, R. Zhu, W. Peng, X. Tan, Early prediction of knee point and knee capacity for fast-charging Lithium-ion battery with uncertainty quantification and calibration, IEEE Trans. Transp. Electrification (2023) 1, https://doi.org/10.1109/tte.2023.3304670, 1.
[29] T. Waldmann, M. Wilka, M. Kasper, M. Fleischhammer, M. Wohlfahrt-Mehrens, Temperature dependent ageing mechanisms in Lithium-ion batteries – a Post-Mortem study, J. Power Sources 262 (2014) 129–135, https://doi.org/10.1016/j.jpowsour.2014.03.112.
[30] L. Wildfeuer, A. Karger, D. Aygül, N. Wassiliadis, A. Jossen, M. Lienkamp, Experimental degradation study of a commercial lithium-ion battery, J. Power Sources 560 (2023), https://doi.org/10.1016/j.jpowsour.2022.232498.
[31] B. Gohla-Neudecker, V.S. Maiyappan, S. Juraschek, S. Mohr, Battery 2 nd life: leveraging the sustainability potential of EVs and renewable energy grid integration. 6th International Conference on Clean Electrical Power (ICCEP), 2017.
[32] Galushkin Ne, N.N. Yazvinskaya, D.N. Galushkin, Mechanism of gases generation during lithium-ion batteries cycling, J. Electrochem. Soc. 166 (2019) A897–A908, https://doi.org/10.1149/2.0041906jes.
[33] L. Geng, D.L. Wood, S.A. Lewis, R.M. Connatser, M. Li, C.J. Jafta, et al., High accuracy in-situ direct gas analysis of Li-ion batteries, J. Power Sources 466 (2020), https://doi.org/10.1016/j.jpowsour.2020.228211.
[34] M. Raghibi, B. Xiong, S. Phadke, M. Anouti, Role of the electrolyte in gas formation during the cycling of a Gr//NMC battery as a function of temperature: solvent, salt, and ionic liquid effect, Electrochim. Acta 362 (2020), https://doi.org/10.1016/j.electacta.2020.137214.
[35] P. Liu, L. Yang, B. Xiao, H. Wang, L. Li, S. Ye, et al., Revealing lithium battery gas generation for safer practical applications, Adv. Funct. Mater. 32 (2022), https://doi.org/10.1002/adfm.202208586.
[36] D. Ren, H. Hsu, R. Li, X. Feng, D. Guo, X. Han, et al., A comparative investigation of aging effects on thermal runaway behavior of lithium-ion batteries, eTransportation 2 (2019), https://doi.org/10.1016/j.etran.2019.100034.
[37] Y. Li, X. Gao, H. Wang, G.J. Offer, S. Yang, Z. Zhao, et al., Direct venting during fast charging of lithium-ion batteries, J. Power Sources 592 (2024), https://doi.org/10.1016/j.jpowsour.2023.233926.
[38] E. Braco, I. San Martín, A. Berrueta, P. Sanchis, A. Ursúa, Experimental assessment of cycling ageing of lithium-ion second-life batteries from electric vehicles, J. Energy Storage 32 (2020), https://doi.org/10.1016/j.est.2020.101695.
[39] E. Braco, I. San Martin, A. Berrueta, P. Sanchis, A. Ursua, Experimental assessment of first- and second-life electric vehicle batteries: performance, capacity dispersion, and aging, IEEE Trans. Ind. Appl. 57 (2021) 4107–4117, https://doi.org/10.1109/tia.2021.3075180.
[40] James. Nissan Leaf 40kWh fried battery teardown and repair. https://www.youtube.com/watch?v=-ySOspbt0BM&t=36s, 2021.
[41] P. Lima, Nissan Leaf battery real specs. 2018. https://pushevs.com/2018/01/29/2018-nissan-leaf-battery-real-specs/, 2018.
[42] X. Hu, S. Li, H. Peng, A comparative study of equivalent circuit models for Li-ion batteries, J. Power Sources 198 (2012) 359–367, https://doi.org/10.1016/j.jpowsour.2011.10.013.
[43] X. Wang, X. Wei, J. Zhu, H. Dai, Y. Zheng, X. Xu, et al., A review of modeling, acquisition, and application of lithium-ion battery impedance for onboard battery management, eTransportation 7 (2021), https://doi.org/10.1016/j.etran.2020.100093.
[44] W. Gao, Y. Zou, F. Sun, X. Hu, Y. Yu, S. Feng, Data pieces-based parameter identification for lithium-ion battery, J. Power Sources 328 (2016) 174–184, https://doi.org/10.1016/j.jpowsour.2016.08.018.
[45] H. Kang, A. Washington, M.D. Capobianco, X. Yan, V.V. Cruz, M. Weed, et al., Concentration-Dependent photocatalytic upcycling of poly(ethylene terephthalate) plastic waste, ACS Mater. Lett. 5 (2023) 3032–3041, https://doi.org/10.1021/acsmaterialslett.3c01134.
[46] W. Gao, X. Li, M. Ma, Y. Fu, J. Jiang, C. Mi, Case study of an electric vehicle battery thermal runaway and online internal short-circuit detection, IEEE Trans. Power Electron. 36 (2021) 2452–2455, https://doi.org/10.1109/tpel.2020.3013191.
[47] M. Uitz, M. Sternad, S. Breuer, C. Täubert, T. Traußnig, V. Hennige, et al., Aging of Tesla's 18650 lithium-ion cells: correlating solid-electrolyte-interphase evolution with fading in capacity and power, J. Electrochem. Soc. 164 (2017) A3503–A3510, https://doi.org/10.1149/2.0171714jes.
[48] Tesla Impact Report. 2023, 2022. https://www.tesla.com/ns_videos/2022-tesla-impact-report.pdf.
[49] M. Dubarry, C. Truchot, B.Y. Liaw, Synthesize battery degradation modes via a diagnostic and prognostic model, J. Power Sources 219 (2012) 204–216, https://doi.org/10.1016/j.jpowsour.2012.07.016.
[50] M. Dubarry, D. Anseán, Best practices for incremental capacity analysis, Front. Energy Res. 10 (2022), https://doi.org/10.3389/fenrg.2022.1023555.
[51] Y. Li, J. Guo, K. Pedersen, L. Gurevich, D.-I. Stroe, Investigation of multi-step fast charging protocol and aging mechanism for commercial NMC/graphite lithium-ion batteries, J. Energy Chem. 80 (2023) 237–246, https://doi.org/10.1016/j.jechem.2023.01.016.